



Original Article

Electrodeposition of CaCO_3 on stainless steel 316 L substrate: influence of thermal-hydraulics and electrochemical parameters

Sid Ahmed Amzert^{a,*}, Fahd Arbaoui^a, Mohamed Nadir Boucherit^b, Noureddine Selmi^a, Salah Hanini^c

^a Nuclear Research Centre of Birine, BO: 180 Ain Oussera, 17200, Djelfa, Algeria

^b Nuclear Engineering Research and Development Unit, BO 399 Algiers, Algeria

^c Yahia Fares University, Ain-D'heb, 26000, Médéa, Algeria

ARTICLE INFO

Article history:

Received 15 March 2021

Revised 12 April 2021

Accepted 14 April 2021

Keywords:

Oxygen reduction reaction;

Stainless steel 316L;

CaCO_3 deposit;

Calcite;

Aragonite.

ABSTRACT

In this paper we study the effect of the hardness, the rotation speed, the temperature and the cathodic polarization on calcium carbonate scale deposit on rotating stainless steel electrode using electrochemical techniques. The scale deposit was investigated by X-Ray diffraction, scanning electron microscope, Infrared spectroscopy and electrochemical impedance spectroscopy (EIS). The electrochemical results show that the Oxygen Reduction Reaction (ORR), which is responsible of CaCO_3 electrodeposition, takes place with 4 electrons at low rotation speed lower than 600 rpm and 2 electrons at high rotation speed upper to 1000 rpm. The recovery times of concentrations: 100, 300 and 600 mg/L are respectively 2.0 h 20 min, 1 h 20 min and 1 h. The morphology of the CaCO_3 scale deposit shows that the crystals formed in the center of the electrode have small sizes compared to those of the periphery. Whatever the hydrodynamic or thermodynamic conditions, the Calcite form remains predominant. Other forms appear in particular conditions: at high temperature up to 50°C the aragonite form and at high cathodic polarization about -1.2 V/SCE the vaterite form.

1. Introduction

In industrial plants, the scale deposit is an undesirable phenomenon that can cause costly damage which could influence the safety aspects in cooling circuits [1]. Scale studies focus mainly on the mechanisms, nature and morphology, of the crystals growth as well as the use of antiscalant chemical substances that inhibit the development [2].

The scale deposit consists mainly of calcium carbonates which precipitates in different crystal structures: aragonite, vaterite, calcite, mono-hydro-calcite and hexa-hydro-calcite [3, 4, 5]. The work of Wang et al. has shown that at room temperature and pressure, calcite is the most stable form while vaterite is the least stable form and easily transforms into one of the other two polymorphs [6].

The formation of these polymorphs depends on many parameters such as chemical composition and

supersaturation, temperature, electric field, magnetic field, foreign ion, organic or inorganic additives and pH [7]. Other parameters can influence the nucleation mechanism of CaCO_3 such as flow velocity, hydrodynamic conditions, materials and surface roughness [8, 9].

The majority of scale deposition studies use the electrodeposition technique [10], by the application of a cathodic potential to a material which provoke oxygen reduction on the surface promoting the oxygen reduction reaction ORR [11]. During cathodic polarization, the active metal surface is progressively blocked by the growth of scale causing a decrease in the current which is proportional to the diffusion of oxygen gas from the bulk solution to the metal surface. The residual current after total surface coverage remains minimal due to diffusion of oxygen gas through the pores of CaCO_3 [12]. By using

* Corresponding author.

E-mail address: samzert@gmail.com

Peer review under responsibility of University of Echahid Hamma Lakhdar.

2716-9227/© 2021 The Authors. Published by University of Echahid Hamma Lakhdar.. This is an open access article under the CC BY-NC license

(<https://creativecommons.org/licenses/by-nc/4.0/>).

<http://dx.doi.org/10.5281/zenodo.4695955>

rotating electrode the diffusion of oxygen gas at the surface of the electrode is governed by the mass transfer, as defined by Levich theory [11].

Two mechanisms are proposed for ORR reaction: mechanism with 2 electrons and 4 electrons according to the state of the surface and the pH of the medium [13]. Whatever the mechanism followed by the ORR reaction, hydroxides are produced, which causes the formation of bicarbonate and carbonate species. With the presence of calcium, the calcium carbonate deposit is formed on the electrode surface [14].

In this study we present the results of electrodeposition of scale on stainless steel 316 L substrate, and we investigate the influence of: the rotation speed, the solution hardness, the cathodic potential polarization and the temperature. The scale layer deposit on stainless steel is obtained by the chronoamperometry and the characterization was carried out by X-ray diffraction, scanning electron microscope and Fourier transform infrared spectrometry techniques. The overall objective of this study is to determine critical parameters affecting the scale deposition for further study.

2. Materials and Methods

2.1. Material

The sample selected for the study was a stainless steel 316L, with chemical composition: Cr 16,55%, Ni 10,06 %, Mo 2,03%, C 0,018% and the remainder is Fe . The sample is coated with Poly Tetra Fluro Ethylene (PTFE) for a rotating disk electrode RDE (exposed surface area is 0.196 cm^2).

2.2. Solution test

Deionized water and analytical reagent grade: sodium chloride, NaCl, The sodium carbonate, Na_2CO_3 , calcium chloride CaCl_2 were used to prepare all solutions and carbon dioxide, CO_2 gas is used by bubbling to dissolve the calcium carbonate precipitate, at a pH below 5.8, to ensure the total solubility of CaCO_3 .

2.3. Electrochemical techniques

Electrochemical tests are conducted in a test cell with three electrodes, the working electrode with a diameter of 5 mm. Its surface is polished with 1200 grade abrasive paper and then rinsed with deionized water, cleaned and degreased with acetone. The reference electrode is a Saturated Calomel Electrode (SCE) and the auxiliary electrode is a platinum sheet. The electrochemical polarization tests were performed using Parstat 2273 model Potentiostat/Galvanostat, and controlled by Powersuite software. In the first step, the Open Circuit Potential (OCP) was recorded for two hours for each solution. The main role of the potentiodynamic polarization is the determination of the oxygen reduction range. Scale deposit

is formed by chronoamperometry. The polarization time was set to two hours. The electrochemical impedance spectroscopy (EIS) measurements were performed at the Open circuit potential: OCP in the frequency range 100 kHz to 100 mHz and with a potential perturbation amplitude of 10 mV.

2.4. X-Ray diffraction

The X-rays diffraction analyzes were carried out by a PANalytical X'Pert Pro-MPD Diffractometer in Bragg-Brentano (θ - θ) configuration mode, equipped with a vertical goniometer with a 240 mm radius and provided by a copper anticathode X ray tube and a window size $20 \times 24 \text{ mm}^2$ Xenon gas detector. The sample holder used is the spinner. The XRD analysis parameters are the following: scan angle from 25 to $65^\circ 2\theta$, step size of $0.02^\circ 2\theta$ and counting time of 1 s.

2.5. Infrared (IR) measurements

Infrared (IR) measurements were carried out by a Fourier transform infrared spectrometer - FTIR (INFRALUM FT-02). All spectra were collected under ambient conditions in the frequency range of 4000 to 400 cm^{-1} with a resolution of 4 cm^{-1} . All spectra were saved and treated by SpectraLum software.

2.6. Scanning Electron Microscopy

The morphologies of scale deposition were investigated by scanning electron microscopy (SEM –Philips XL 30 microscope coupled to an energy dispersive analyzer (EDX).

3. Results and Discussion

It is important to determinate the OCP of electrode which is controlled by oxidation and reduction reactions of metal in the solution.

Figure 1 shows the OCP evolution of a rotating electrode of stainless steel 316L in aerated solution containing: Na_2CO_3 300 mg/L, NaCl 10^{-2} mole/L at pH equal 10.6 at different rotation speeds during 2 hours. OCP is recorded between -0.385 and -0.450 V/SCE. It can see, after 2 hours the OCP evolves anodically according to the rotation speed. This indicates the increase of cathodic reaction. The rotation speed ensures the transport of dissolved oxygen to the surface of the electrode.

This favors the reduction reactions which generates a greater cathode current and therefore an anodic displacement of E_{corr} . Whatever the rotation speed of the electrode, the anodic evolution of the OCP is limited by the formation of the passive film on the surface of the electrode [15].

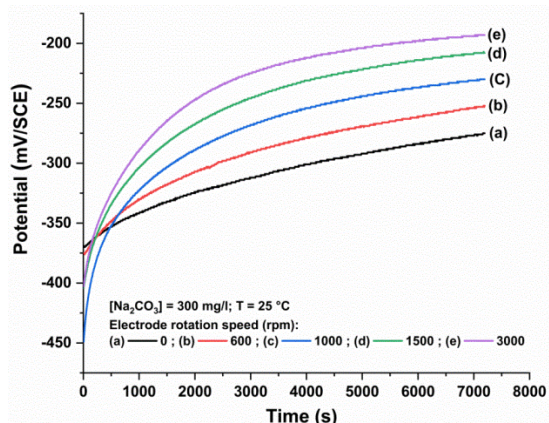


Fig 1. OCP evolution of RDE in Na_2CO_3 solution.

In Figure 2 the cathodic polarization curves $I = f(E)$ between OCP and $-1.8 \text{ V} / \text{SCE}$, of electrode have been obtained with a scan rate of 1 mV/s in a solution containing: Na_2CO_3 300 mg/L , NaCl 10^{-2} mole/L at several rotation speed and at $\text{pH} = 11.5$ and 5.4 .

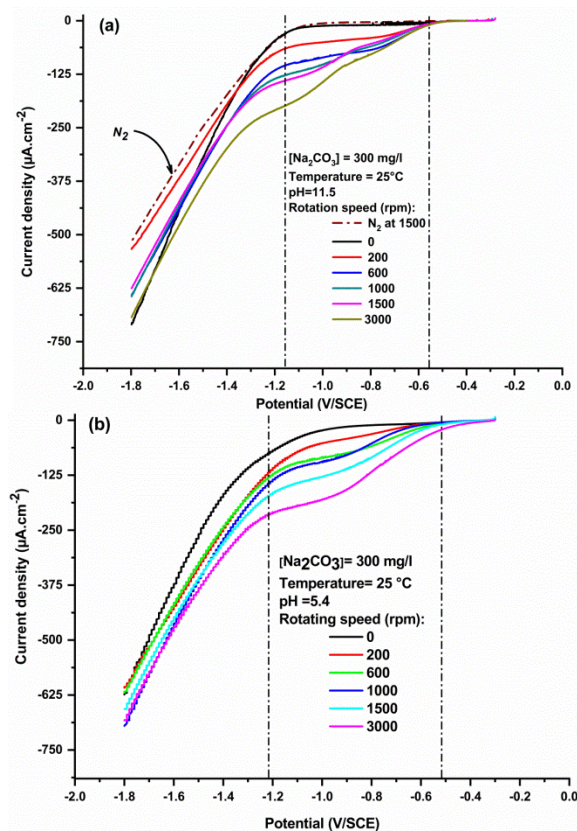


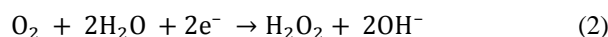
Fig 2. Potentiodynamic curve of RDE immersed in Na_2CO_3 and NaCl at : (a) $\text{pH} = 11.5$ and (b) $\text{pH} = 5.4$.

In Figure 2 (a) and (b), the cathodic currents increase with the rotation speed. This allows more dissolved oxygen to be supplied to the surface of the electrode. In Figure 2(a), at rotation speed 1500 rpm with nitrogen bubbling,

we there is no cathodic current between -0.5 and -1.2 V/SCE . Without nitrogen bubbling, which means in the presence of oxygen, two peaks of cathodic currents are observed. They correspond to oxygen reduction reactions. At high pH , in Figure 2 (a), there are one cathodic current peak for low rotation speeds and two current peaks for rotation speeds above 1000 rpm . These peaks are located around -0.8 and $-1 \text{ V} / \text{SCE}$. At low pH , Figure 2 (b), only a single peak of cathodic current exist regardless the rotation speed of the electrode. This difference in behavior observed at different pH is explained by the fact that in an alkaline medium the reduction of oxygen occurs according to the reaction with 4 electrons: (Eq.1) [16]:



For high rotation speed the reduction takes place in two peaks according to the reactions (Eq.2) and (Eq.3) [17]:



While in an acidic medium $\text{pH} = 5.4$, the reduction of oxygen is done in a single stage with 4 electrons following the reaction (Eq.4) [18]:



Whatever the pH of solution, the increase of cathodic current up to -1.2 V/SCE , comes from the contribution of the water reduction reaction according to (Eq.5) [19]:



To explain the effect of rotation speed on the oxygen reduction current and the dependence of cathodic reactions on the oxygen diffusion factor, the linearity of the reciprocal of current with the reciprocal of square root of the rotation speed $I^{-1} = f(\omega^{-1/2})$ was verified, this illustration corresponds to Koutecky–Levich equations [20]:

$$\frac{1}{j} = \frac{1}{j_{\text{lim}}} + \frac{1}{j_{\text{K}}} = \frac{1}{B\sqrt{\omega}} + \frac{1}{j_{\text{K}}} \quad (6)$$

Where, j_{K} is the kinetic current density; j_{lim} the diffusion-limiting current density; j the measured current density; B the reciprocal of the slope; ω the electrode rotation speed.

$$B = 0,621 n_e F A C_A D_A^{2/3} \nu^{-1/6} \quad (7)$$

Where n_e is number of electrons transferred during the reaction, F is the Faraday constant ($96485.34 \text{ C}\cdot\text{mol}^{-1}$), A area of the electrode, C_A and D_A the concentration (Mole/L) and the diffusion coefficient ($\text{m}^2\cdot\text{s}^{-1}$) of the electroactive species in our case oxygen, ω is the rotation speed ($\text{rad}\cdot\text{s}^{-1}$) and ν is the kinematic viscosity of the electrolyte ($\text{m}^2\cdot\text{s}^{-1}$).

Figure 3 presents the intensity of the cathodic current taken from the peak of ORR as a function of the square root of the electrode rotation speed. For precision, current value corresponding to the middle of the current peak ORR was recorded. This series of measurements is made at several temperatures.

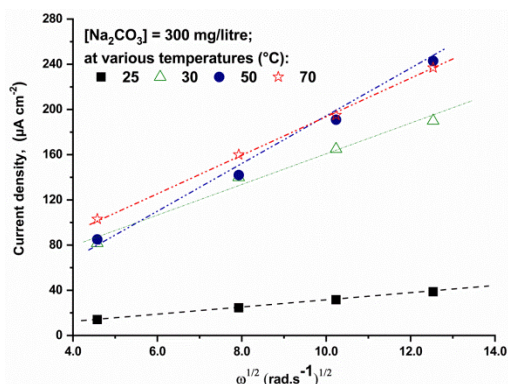


Fig 3. Levich curves deduced from cathodic polarization curves at various temperature and rotation speed.

The current density evolves linearly with the square root of the speed of rotation for each temperature. This shows that the ORR is controlled by mass transport and temperature parameters.

In the following, the influences of thermohydraulics and chemical parameters on the quality of scale deposits were studied using chronoamperometry technique. Figure 4 shows the evolution over time of the current density for CaCO_3 concentration between 50 and 600 mg/L at 25 °C, 600 rpm and polarization at a potential of -1 V/SCE. It can be seen that the increase of CaCO_3 concentration reduces the recovery time t_s , and the residual current I_r (as shown in Figure 4).

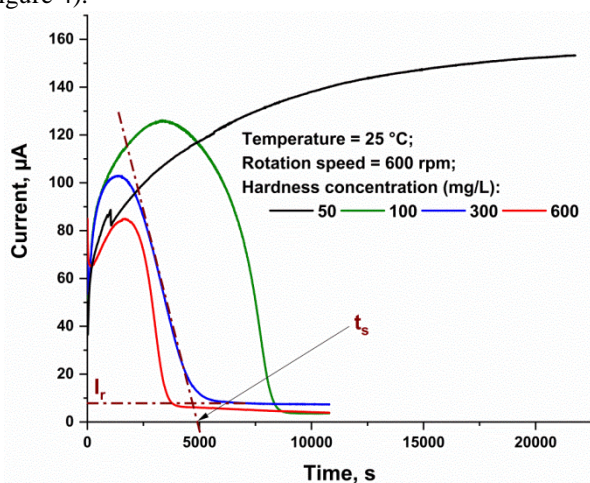


Fig 4. Chronoamperometric curves of RDE at various CaCO_3 concentrations.

The recovery time for: 100, 300 and 600 mg/L concentrations are respectively 2.0 hrs: 20 min, 1.0 hr: 20 min and 1.0 hr. For 50 mg/L of CaCO_3 , the cathodic current increases slightly but continuously, this means that the surface of RDE is not covered with scale deposit. For higher hardness, a rapid fall of cathodic current is observed which indicates a total surface coverage. The maximum current recorded is inversely proportional to the hardness due to the inhibition of ORR reaction.

The deposit formed on the surface of the RDE was examined by the X-ray diffraction technique shown in Figure 5. The XRD pattern obtained showed the presence of two forms of CaCO_3 : calcite a predominant form, and a small proportion of aragonite. In addition, to peaks of the electrode materials which correspond to Steel (SS) and Teflon (T).

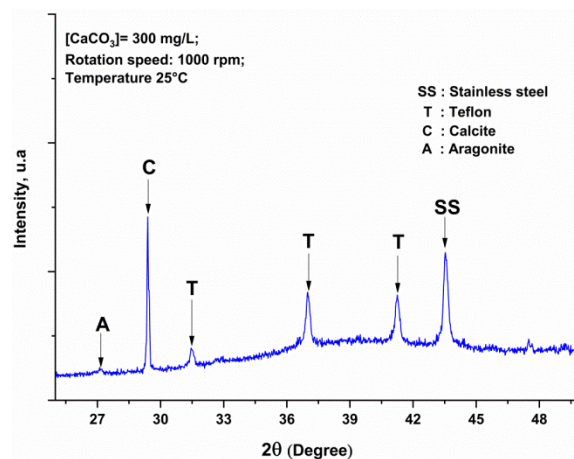


Fig 5. X-ray diffraction pattern of scale formed on stainless steel surface.

The XRD analysis was accompanied by an infrared FTIR analysis. The spectrum shown in Figure 6 was obtained by analyzing a scale deposit made at 25 °C.

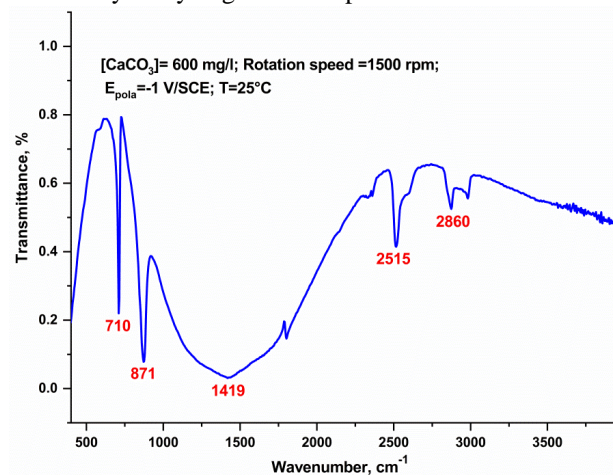


Fig 6. Fourier-transform infrared (FTIR) spectra of CaCO_3 scale deposit.

The vibrational peaks located at 710, 871 and 1419 cm^{-1} correspond to calcite according to [22, 23]; 1419 cm^{-1} stretching mode of C-O, 870 cm^{-1} narrow band of bending mode, 710 cm^{-1} bending the mode in plane of O-C-O and the symmetric and asymmetric stretching vibration of O-C-O at 2515 cm^{-1} . The two frequencies at 2515 and 2860 cm^{-1} correspond to the C-H and O-H bonds. The presence of these peaks is probably due to impurities and low humidity [24].

Figure 7 presents the chronoamperometry curves of RDE at several rotation speeds at 25 °C, 300 mg/L of CaCO_3 and at -1 V / SCE. It was noted that the recovery time is proportional to the rotation speed. When the solution is stagnant, the residual current is about 25 μA . For rotation speeds of 600 and 1500 rpm, it is observed that the residual current becomes weaker.

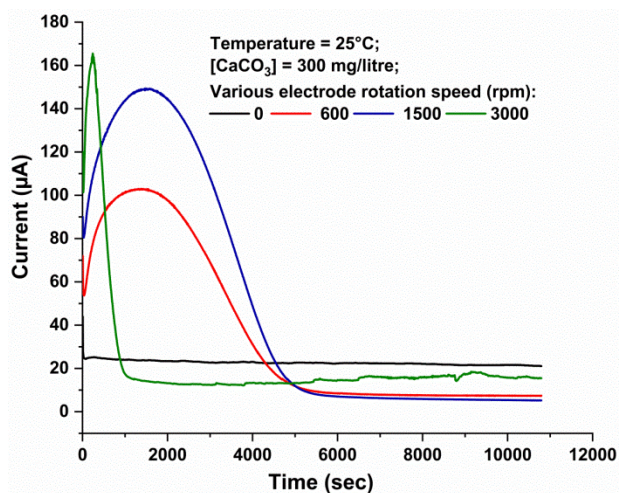


Fig 7. Chronoamperometric curves of RDE at various CaCO_3 rotation speed.

At a higher rotation speed, the residual current is reached faster, but it increases over the recorded currents of the 600 and 1500 rpm speeds and it remains lower than the residual current in a stagnant solution. A high rotation speed could tear off pieces of scale deposit from deposit layers, and therefore the growth and morphology of the scale deposit is affected.

For a rotation speed of 1500 rpm, morphology of the deposit formed at the center and at the periphery of RDE was examined as illustrated in Figure 8.

It is observed that at the center of the electrode, the crystals are smaller and have irregular shapes, at the periphery the crystals are much larger and have parallelepipedal shapes. This difference is explained by the diffusion of hydroxide ions, produced by the reduction of oxygen, centrifugally under the effect of the rotation of the electrode. This creates a decreasing pH gradient from the center to the periphery of the surface. This pH gradient is the origin of the initiation points of scale depositing germs decreasing moving away from the center [25].

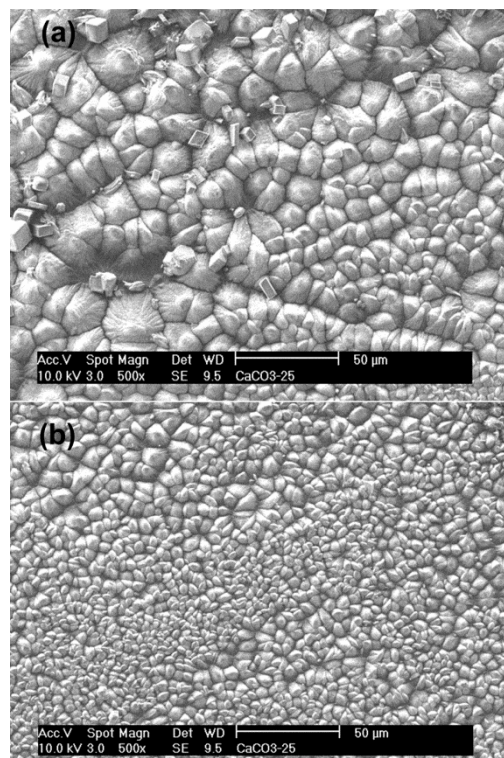


Fig 8. Morphology of scale deposit at center and periphery of RDE at 25 °C, 1500 rpm and -1 V/SCE polarization potential.

To further characterize the scale deposit, we used the electrochemical impedance spectroscopy. The Nyquist plots for each rotation speed of stainless steel covered by scale deposit at the OCP potential after chronoamperometry test at 25°C are presented in Figure 9.

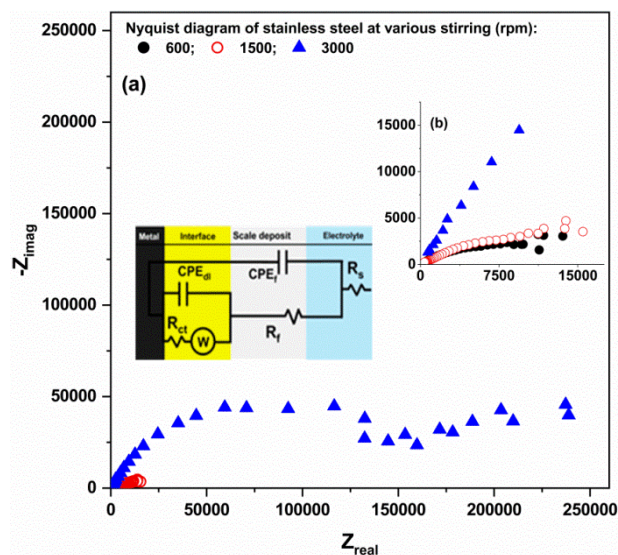


Fig 9. Nyquist plots of electrode covered by scale deposit at various rotation speeds at OCP and 25 °C (b) zoom of Nyquist plot at low Z_{real} .

Nyquist curves are not perfect semicircles. The responses of the impedance data were modelled using an electrical equivalent circuit presented in Figure 9. This circuit consists of two RC loops. The first loop corresponds to the charge transfer reactions. R_{ct} : resistance of the charge transfer corresponding to the reduction of dissolved oxygen and CPE_{dl} is related to the double layer capacitance. The second loop consists of the capacitance CPE_f which represents the isolation imposed by the scale deposit crystals and a resistance R_f which represents the resistance of scale deposit crystals. W is the diffusion impedance through the scale deposit. Finally, the resistance R_s describes the resistance of the solution between the working electrode and the reference electrode. The results of the EIS data fitted with the Zsimpwin software are presented in Table 2, where χ^2 is the error factor. The modelling error factor χ^2 does not exceed 5%. The resistances of the scale deposit R_f for the two speeds 600 and 1500 rpm are quite close to 8.53 and 9.23 kOhm respectively, unlike, for the rotation speed 3000 rpm the resistance is 138.4 kOhm, at a high rotation speed, promoting the tearing of crystals formed on the surface by creating pores where resistance is important comparatively to other rotation speeds.

Table 1. Fitting results for the EIS data of stainless steel covered by scale deposit at various rotation speed.

		Rotation speed (rpm)		
		600	1500	3000
R_s	Unit			
	KOhm	0.20	0.16	0.12
CPE_f	$\mu F.s^{(n-1)}$	9.38	20.01	0.06
n_f		0.47	0.39	0.71
R_f	KOhm	8.53	9.23	138.42
CPE_{dl}	$\mu F.s^{(n-1)}$	8.70	0.08	6.00
n_{dl}		0.99	1	0.49
R_{ct}	KOhm	2.21	6.15	205.63
W	$KOhm.s^{0.5}$	2.19	4.07	0.15
χ^2		0.011	0.023	0.022

This explication has an implicit influence in the same way on the resistance of the double layer where the value of the resistance at 3000 rpm is significant 205.6 KOhm compared to the 600 and 1500 rpm.

As it was explained in the illustration of Levich the temperature is a parameter which is involved in the kinetics and transport of the ORR. Figure 10 presents the effect of temperature at 25, 30, 40 and 70 °C, on current evolution over time by fixing the $CaCO_3$ concentration at 300 mg/L and a rotation speed of 600 rpm and at a polarization potential of -1 V / SCE.

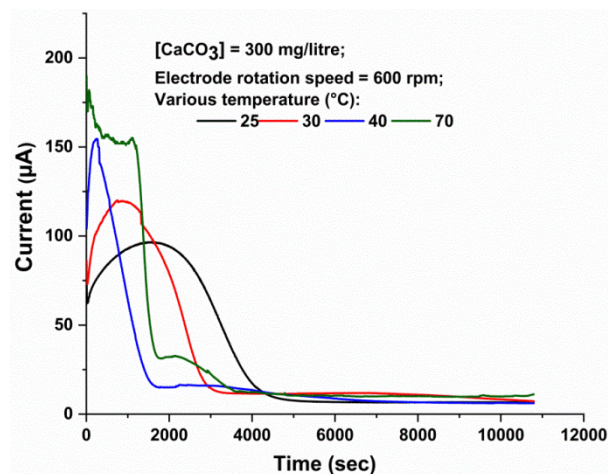


Fig 10. Chronoamperometric curves of RDE at various temperature of solution.

In this Figure, a drop in the current which depends on the temperature after a period of polarization is observed, showing a covering of the surface by a scale deposit. However, it can be seen that at 40° and 70° C curves, the current drop occurs in two steps. The first peak appears after half an hour of polarization, then continues until it reaches the second peak which corresponds to the residual current regardless of temperature. For lower temperatures these observations are much less obvious.

For an accurate examination of the deposits at different temperatures, the surfaces were analyzed by XRD as shown in Figure 11. The scale deposit contains calcite and aragonite forms for all temperatures. It can be observed that the calcite / aragonite ratio decreases with increasing temperature.

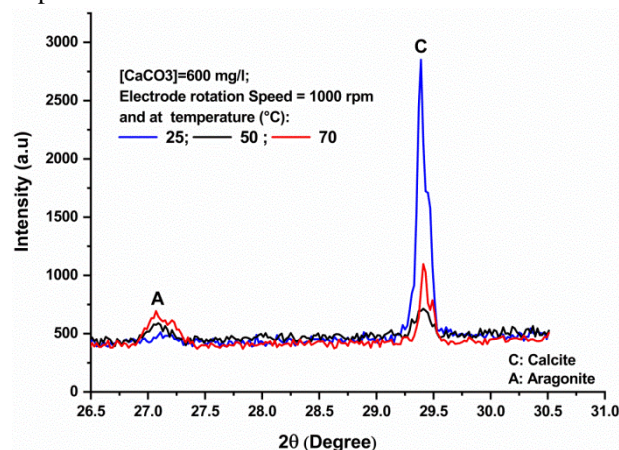


Fig 11. X-ray diffraction pattern of scale deposit formed on stainless steel surface at various temperatures: 25, 50 and 70 °C.

The morphology of deposit scale at 25 and 70 °C was examined using SEM technique (Figure 12). The main difference between these two deposits morphologies is the

shape of the crystals. At 25 ° C the deposit is rhombohedral which characterizes the calcite presented in figure 12 (a).

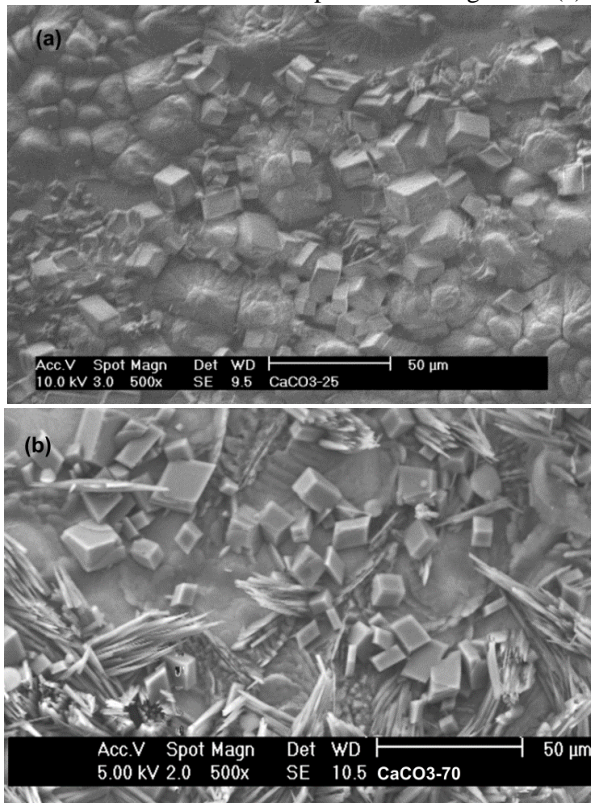


Fig 12. Morphology of scale deposit at (a):25°C and (b): 70°C.

While at 70 ° C, calcium carbonates crystallize in the elongated form known as aragonite. The scale deposit formed at 70 ° C also contains calcite as illustrated in Figure 12 (b).

Figure 13 illustrates the effect of the variation of cathodic polarization, on current versus time by fixing the CaCO_3 concentration at 300 mg/L and a rotation speed of the electrode of 600 rpm and at temperature of 25°C.

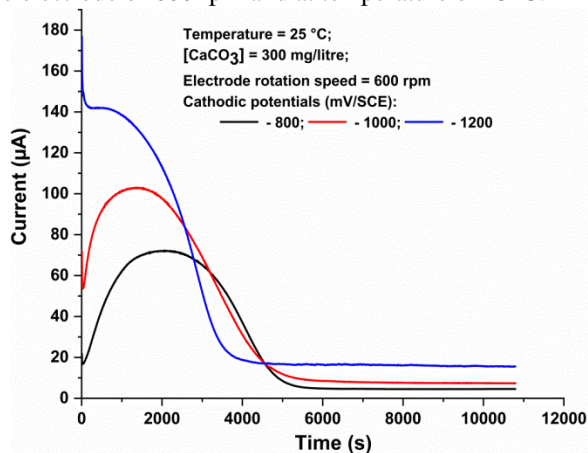


Fig 13. Chronoamperometric curves of electrode at various potentials of polarization.

As it can be seen from figure 13, at the start of the experiments the recorded current is related to the applied

cathode potential. For polarizations at - 0.800 and -1 V / SCE, the recorded current goes through a maximum with the same recovery time, unlike a polarization at -1.2 V / SCE where it can be observed a progressive decrease in the current and a recovery time less than the two previous experiences. The residual current recorded at -1.2 V / SCE is greater than that observed for - 0.800 and -1 V / SCE. At more cathodic potentials water reduction (Eq. 5) contributes also to the current. This explains the high value of the current generated at -1.2 V / SCE. The hydrogen molecules produced from water reduction to a potential of - 1.2 V / SCE disrupts the formation of an adherent and compact deposit on electrode surface which results in a high residual current compared to less cathodic polarizations [26].

Figure 14 presents the morphology of the deposit formed at -1.2 V / SCE.



Fig 14. Surface morphology of scale deposit at -1.2 V/SCE.

On this Figure14, it can be seen a major presence of aragonite with calcite and a third species of CaCO_3 in the form of a flower called vaterite according to the literature [27].

4. Conclusion

The analysis of all experimental data presented in this work leads to the following conclusions concerning the effect of thermohydraulics and electrochemical parameters on the scale deposition on RDE of stainless steel 316L. The results of electrochemical experiments have shown that the rotation speed further promotes the transport of oxygen gas to the surface of the electrode where the Oxygen Reduction Reaction will take place. The oxygen reduction which is responsible of CaCO_3 electrodeposition takes place with 4 electrons at low rotation speed and 2 electrons at high speed in the range -800 and -1000 mV / SCE. The results of (EIS) show that at high rotation speed 3000 rpm the resistance R_f and R_{ct} are high respectively 138.4 And 205.6 kOhm compared to 600 and 1500 rpm. At more cathodic

potentials -1.2 V/SCE, the water reduction reaction releases hydrogen gas which disrupts the nucleation of the scale the residual current recorded is about $18\mu\text{A}$. The XRD and SEM results show a main presence of calcite at room temperature. The proportion of aragonite increases with increasing temperature. The results also showed that vaterite appears at more cathodic polarization.

Acknowledgements

This work was supported by the Nuclear Research Centre of Birine, Algeria.

Conflict of Interest

The authors declare that they have no conflict of interest

References

1. Pečnik B, Hočevnar M, Širok B, Bizjan B. Scale deposit removal by means of ultrasonic cavitation. *Wear*. 2016 Jun 15;356:45-52.
2. Zuo Z, Yang W, Zhang K, Chen Y, Li M, Zuo Y, Yin X, Liu Y. Effect of scale inhibitors on the structure and morphology of CaCO_3 crystal electrochemically deposited on TA1 alloy. *Journal of colloid and interface science*. 2020 Mar 7;562:558-66.
3. Jimoh OA, Ariffin KS, Hussin HB, Temitope AE. Synthesis of precipitated calcium carbonate: a review. *Carbonates and Evaporites*. 2018 Jun 1;33(2):331-46.
4. Cuesta Mayorga I, Astilleros JM, Fernández-Díaz L. Precipitation of CaCO_3 polymorphs from aqueous solutions: The role of pH and sulphate groups. *Minerals*. 2019 Mar;9(3):178.
5. Blue CR, Dove PM. Chemical controls on the magnesium content of amorphous calcium carbonate. *Geochimica et Cosmochimica Acta*. 2015 Jan 1;148:23-33.
6. Chen SF, Yu SH, Jiang J, Li F, Liu Y. Polymorph discrimination of CaCO_3 mineral in an ethanol/water solution: Formation of complex vaterite superstructures and aragonite rods. *Chemistry of Materials*. 2006 Jan 10;18(1):115-22.
7. MacAdam J, Parsons SA. Calcium carbonate scale formation and control. *Re/Views in Environmental Science & Bio/Technology*. 2004 Jun 1;3(2):159-69.
8. Wang LC, Li SF, Wang LB, Cui K, Zhang QL, Liu HB, Li G. Relationships between the characteristics of CaCO_3 fouling and the flow velocity in smooth tube. *Experimental Thermal and Fluid Science*. 2016 Jun 1;74:143-59.
9. Liu Y, Zou Y, Zhao L, Liu W, Cheng L. Investigation of adhesion of CaCO_3 crystalline fouling on stainless steel surfaces with different roughness. *International Communications in Heat and Mass Transfer*. 2011 Jul 1;38(6):730-3.
10. Lédion J, Leroy P, Labbé JP. Détermination du caractère incrustant d'une eau par un essai d'entartrage accéléré. *Techniques et sciences municipales* (1971). 1985(7-8):323-8.
11. Neville A, Hodgkiess T, Morizot AP. Electrochemical assessment of calcium carbonate deposition using a rotating disc electrode (RDE). *Journal of applied electrochemistry*. 1999 Apr;29(4):455-62.
12. Chen T, Neville A, Yuan M. Calcium carbonate scale formation—assessing the initial stages of precipitation and deposition. *Journal of Petroleum Science and Engineering*. 2005 Mar 15;46(3):185-94.
13. Gómez-Marín AM, Rizo R, Feliu JM. Oxygen reduction reaction at Pt single crystals: a critical overview. *Catalysis Science & Technology*. 2014;4(6):1685-98.
14. Tlili MM, Benamor M, Gabrielli C, Perrot H, Tribollet B. Influence of the interfacial pH on electrochemical CaCO_3 precipitation. *Journal of the Electrochemical Society*. 2003 Sep 19;150(11):C765.
15. Wang Z, Seyeux A, Zanna S, Maurice V, Marcus P. Chloride-induced alterations of the passive film on 316L stainless steel and blocking effect of pre-passivation. *Electrochimica Acta*. 2020 Jan 1;329:135159.
16. Le Bozec N, Compère C, L'Her M, Laouenan A, Costa D, Marcus P. Influence of stainless steel surface treatment on the oxygen reduction reaction in seawater. *Corrosion science*. 2001 Apr 1;43(4):765-86.
17. Devos O, Gabrielli C, Tribollet B. Simultaneous EIS and in situ microscope observation on a partially blocked electrode application to scale electrodeposition. *Electrochimica acta*. 2006 Jan 20;51(8-9):1413-22.
18. Muthukrishnan A, Nabae Y, Hayakawa T, Okajima T, Ohsaka T. Fe-containing polyimide-based high-performance ORR catalysts in acidic medium: a kinetic approach to study the durability of catalysts. *Catalysis Science & Technology*. 2015;5(1):475-83.
19. Neville A, Morizot AP. Calcareous scales formed by cathodic protection—an assessment of characteristics and kinetics. *Journal of Crystal Growth*. 2002 Sep 1;243(3-4):490-502.
20. Xu S, Kim Y, Higgins D, Yusuf M, Jaramillo TF, Prinz FB. Building upon the Koutecky-Levich equation for evaluation of next-generation oxygen reduction reaction catalysts. *Electrochimica Acta*. 2017 Nov 20;255:99-108.
21. Srbac S. The effect of pH on oxygen and hydrogen peroxide reduction on polycrystalline Pt electrode. *Electrochimica Acta*. 2011 Jan 1;56(3):1597-604.
22. Chen J, Xiang L. Controllable synthesis of calcium carbonate polymorphs at different temperatures. *Powder Technology*. 2009 Jan 25;189(1):64-9.
23. Li J, Yang S, Liu Y, Muhammad Y, Su Z, Yang J. Studies on the properties of modified heavy calcium carbonate and SBS composite modified asphalt. *Construction and Building Materials*. 2019 Sep 10;218:413-23.
24. Islam KN, Bakar MZ, Ali ME, Hussein MZ, Noordin MM, Loqman MY, Miah G, Wahid H, Hashim U. A novel method for the synthesis of calcium carbonate (aragonite) nanoparticles from cockle shells. *Powder Technology*. 2013 Feb 1;235:70-5.
25. Amzert SA, Hanini S, Boucherit MN. Influence of permanganate reduction on CaCO_3 crystals' growth on a rotating metal surface. *Journal of crystal growth*. 2013 Nov 1;382:15-20.
26. Piri M, Arefinia R. Investigation of the hydrogen evolution phenomenon on CaCO_3 precipitation in artificial seawater.

Desalination. 2018 Oct 15;444:142-50.

27. Huang JH, Mao ZF, Luo MF. Effect of anionic surfactant on vaterite CaCO₃. Materials Research Bulletin. 2007 Dec 4;42(12):2184-91.

Recommended Citation

Amzert SA, Arbaoui F, Boucherit MN, Selmi N, Hanini S. Electrodeposition of CaCO₃ on stainless steel 316 L substrate: influence of thermal-hydraulics and electrochemical parameters. *Alger. J. Eng. Technol.* 2021, 4:90-98. <http://dx.doi.org/10.5281/zenodo.4695955>



This work is licensed under a [Creative Commons Attribution-NonCommercial 4.0 International License](https://creativecommons.org/licenses/by-nc/4.0/)